THE ASTROPHYSICAL JOURNAL, 477:495–501, 1997 March 1

THE IONIC CHARGE OF SOLAR ENERGETIC PARTICLES WITH ENERGIES OF 0.3–70 MeV PER NUCLEON

M. OETLIKER, B. KLECKER, AND D. HOVESTADT
Max-Planck-Institut für extraterrestrische Physik, D-85740 Garching, Germany
G. M. MASON AND J. E. MAZUR
University of Maryland, College Park, MD 20742
R. A. LESKE AND R. A. MEWALDT
California Institute of Technology, Pasadena, CA 91125
AND
J. B. BLAKE AND M. D. LOOPER
The Aerospace Corporation, El Segundo, CA 90245
Received 1996 March 27; accepted 1996 September 16

ABSTRACT

With the three particle sensors Low Energy Ion Composition Analyzer (LICA), Heavy Ion Large Area Proportional Counter Telescope (HILT), and Mass Spectrometer Telescope (MAST) on board the polar-orbiting *Solar, Anomalous, and Magnetospheric Particle Explorer* (*SAMPEX*) satellite, the ionic charge of solar energetic particles (SEP) was measured over a wide energy range from 0.3 to 70 MeV per nucleon. For each sensor, the evaluation was performed separately. The results obtained with LICA (0.3–10 MeV per nucleon) and MAST (15–70 MeV per nucleon) were published earlier by Mason et al. and Leske et al., respectively. In this work we present the results of the HILT sensor (7–50 MeV per nucleon) and discuss the combined results of the three instruments.

With HILT, the mean ionic charge of SEP was measured for carbon, nitrogen, oxygen, neon, magnesium, silicon, sulfur, argon, calcium, and iron in the energy range 7–50 MeV per nucleon during two consecutive large SEP events in 1992 October–November. The mean ionic charge was inferred from the rigidity-dependent geomagnetic flux cutoff. The coronal temperatures deduced from the mean ionic charges are well in accordance with the value of $\sim 2 \times 10^6$ K except for neon and magnesium, as previously reported.

The data measured with the three sensors, LICA, HILT, and MAST, agree well and are in accordance with data previously measured at energies below 3 MeV per nucleon (Luhn et al.), except for iron, where we observed a significant energy dependence of the mean charge over the energy range 0.3–70 MeV per nucleon.

Subject headings: Sun: corona — Sun: flares — Sun: particle emission

1. INTRODUCTION

The ionic charge of solar energetic particles (SEP) observed in interplanetary space is an important parameter for the diagnosis of the plasma conditions at the source of the SEP in the solar corona. The charge is established through temperature-dependent ionization and recombination processes in the corona. When particles emerge from the Sun, the plasma density decreases rapidly, and the charge states "freeze in." The charge state distribution of the SEP therefore reflects the source conditions such as the electron temperature in the corona. By observing the charge of SEP, answers to the following questions can be probed: (1) Do all elements freeze in at the same coronal temperature, (2) is the measured SEP charge independent of the particle energy and therefore not altered by the acceleration processes, and (3) can we observe a variation of the ionization temperature with observed SEP event (e.g., a difference between short- and long-duration events)?

Prior to the *Solar, Anomalous, and Magnetospheric Particle Explorer* (*SAMPEX*), the mean ionic charge of SEP was measured for carbon, nitrogen, oxygen, neon, magnesium, silicon, sulfur, and iron with energies 0.1–3 MeV per nucleon (Gloeckler et al. 1981; Hovestadt et al. 1981; Luhn et al. 1984). These measurements revealed an incomplete ionization of SEP, which indicated a common source temperature around $\sim 2 \times 10^6$ K, but with a much higher value for neon and magnesium. Low charge states, such as C^{+1-3}, O^{+1-4}, and Fe^{+1-5}, were not observed. It was also found that the mean charges are different in SEP events with anomalous composition (e.g., ^{3}He- and heavy ion–rich; Klecker et al. 1983, 1984; Luhn et al. 1987). Recently, the charge of Fe in large gradual SEP events was measured at 200–600 MeV per nucleon by Tylka et al. (1995).

Previous data for the ionic charge of low-energy SEP were obtained with sensors using electrostatic deflection. Such measurements could be made only up to energies of ~ 2 MeV per nucleon. At higher energies, the magnetosphere can be used as a magnetic spectrometer (rigidity separator), and the SEP charge can be determined from the particle penetration depth into the magnetosphere, i.e., the geomagnetic cut-off. The near polar–orbiting *SAMPEX* satellite with its four particle sensors is an ideal platform to observe geomagnetic cutoffs over a wide range of energy. Data were obtained with LICA, HILT, and MAST simultaneously in two consecutive SEP events during the time period 1992 October 30–November 7, covering the wide energy range 0.3–70 MeV per nucleon.

In the first part of this work, we describe the HILT sensor, the method used to determine the charge states, and the results for HILT. In the second part, we combine the

results of the three sensors and discuss the observations.

2. INSTRUMENTATION

SAMPEX was launched in 1992 July. With the near-polar orbit at an inclination of 82° and altitude of 520 × 670 km, *SAMPEX* covers a wide range of magnetic latitudes. The satellite is equipped with four particle detectors, LICA (Low Energy Ion Composition Analyzer), HILT (Heavy Ion Large Area Proportional Counter Telescope), MAST (Mass Spectrometer Telescope), and PET (Proton/Electron Telescope), covering an energy range of 200 keV per nucleon up to >100 MeV per nucleon from H to Fe. For a detailed description of *SAMPEX* and its instruments, see Baker et al. (1993), Klecker et al. (1993), Mason et al. (1993), and Cook et al. (1993a, 1993b).

The HILT sensor combines a stopping power with a residual energy measurement to determine the nuclear charge and the energy of incoming particles. The energy range is 4–30 MeV per nucleon for He, 8–75 MeV per nucleon for O, and 10–150 MeV per nucleon for Fe. A classification scheme identifies four classes of events (two for helium and two for heavy elements) and transmits for each class the total count rate along with five to 10 pulse height–analyzed events per second, from which the absolute flux for particles of a given species and energy can be calculated.

With PET, protons and helium are measured from 20 to 300 MeV per nucleon using a combined dE/dx-total energy technique with eight Li-drifted silicon detectors. One proton channel of this sensor (PLO; 19–28 MeV) was used for normalization purposes. In LICA, a time-of-flight and a residual energy measurement are combined to determine the mass and energy of helium to nickel ions with energies 0.2–10 MeV per nucleon. In MAST, stopping power versus residual energy measurements are used to deduce the mass, nuclear charge, and energy of helium to nickel ions with energies 10–200 MeV per nucleon.

3. METHOD

The magnetosphere is a practical tool for measuring the ionic charge of SEP. The penetration depth of ions into the magnetosphere depends on their gyroradius. On a polar-orbiting spacecraft, moving from a pole to the equator, this can be observed as a flux cutoff of particles of a given magnetic rigidity at a certain magnetic L-shell (or invariant latitude λ). Above a few MeV per nucleon, the inverse square of this magnetic cutoff L-shell value is linearly dependent on the particle's rigidity (Smart & Shea 1994), which can in principle be used to determine the mean charge of the particles.

Flux versus L profiles are accumulated for several energy bins of each particle species over many orbits of the satellite in order to provide sufficient counts in each profile for deducing the cutoff. For each pass between a pole and the equator, the fluxes are normalized with the polar flux of the PLO protons measured with the PET sensor, and the L-values are scaled with the cutoff L-value of the protons in order to correct for the large particle flux variations and magnetic disturbances during the SEP events, respectively. The accumulated profiles are smoothed with a running average, and the cutoff is defined here as 50% of the polar flux in each profile. The mean charges of the heavy elements are then calculated by comparing their cut-off values with the proton cutoff. The ionization temperatures are derived from the mean charges with tables given by Arnaud & Rothenflug (1985) and Arnaud & Raymond (1992).

The 19–28 MeV PLO proton channel of the PET instrument provides sufficient count statistics to determine the magnetic cutoff of the protons for each pass between a pole and the equator (several hundred to several thousand counts). For each pass, the mean polar flux (averaged for $L > 6$), F_P, and the cutoff, L_{C_P} of the protons is determined and is used to normalize the flux, F, and cutoff, L, of the heavy elements. The cutoff L_{C_P} is determined at 50% of F_P in the proton flux-L profiles. In Figure 1, F_P (*upper panel*; for comparisons, polar fluxes of O and Fe measured with LICA and MAST are included in the graph) and L_{C_P} (*lower panel*) are displayed for the time period 1992 October 31–November 7.

The flux, F_{ij}, of the heavy ions measured with HILT is determined for 10 energy bins, j, for each element, i, from pulse height–analyzed events every 6 s. For each pass between a pole and the equator, the flux is computed as a function of L. We exclude data accumulated during the passage through the South Atlantic Anomaly as well as during times when the HILT rates were saturated and dead-time corrections could no more be applied.

During periods with high particle fluxes, HILT measurements can be accumulated only at low latitudes because of saturation effects at high latitudes, resulting in partial $F(L)$-profiles. For particles with high rigidity, such as iron, which reach the lowest L-shells, data can still be accumulated up to the cutoff. These partial $F(L)$-profiles with data gaps for high L add to the shape of the summed profile around the cutoff but do not contribute to the level of the polar flux. Because almost all the counts of most of the elements are accumulated during the high-flux periods, it is important to include the partial profiles in the evaluation to achieve a well defined cutoff. We therefore normalize the fluxes, F_{ij}, with the proton flux, F_P, and average the profiles over an extended time period, omitting the saturation gaps in the individual profiles.

The normalized profiles, $f_{ij}(L) = F_{ij}(L)/F_P$, have to be corrected in terms of L as well, in order to account for

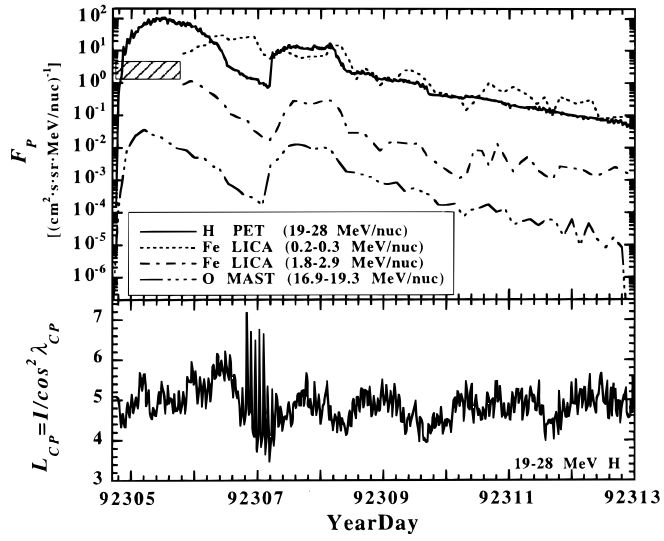

FIG. 1.—*Upper panel*: Mean polar flux (for $L > 6$), F_P, of the PET PLO protons for the time period 1992 October 31–November 7. Also included are polar fluxes of O and Fe measured with LICA and MAST (LICA was off during the hatched interval). *Lower panel*: Cutoff, L_{C_P}, of the PET PLO proton channel for the same time period.

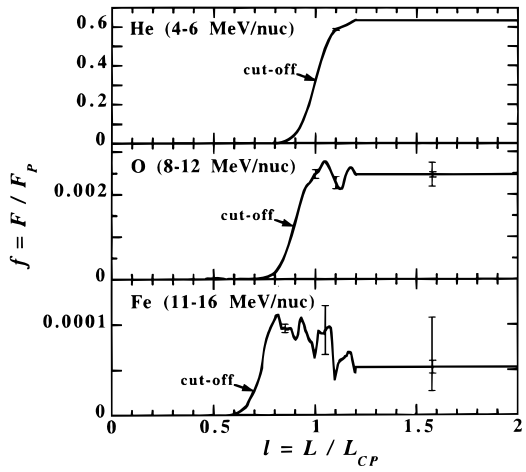

FIG. 2.—Examples of smoothed $f_{ij}(l)$-profiles for the lowest energy bins of helium, oxygen, and iron, accumulated with the HILT sensor from 1992 October 31 to November 7. Beyond $l = 1.2$, the value for the polar flux is plotted, showing the estimated range of statistical and systematic error arising from instrument saturation effects that are particularly important for Fe.

the variation of the cutoff, $L_{C_{ij}}$, in the disturbed magnetosphere during SEP events, as well as asymmetries of the magnetosphere. The cutoff values vary up to $\pm 20\%$ from pass to pass (see Fig. 1). The correction is implemented by dividing the L-scale by L_{C_P}, assuming a constant ratio between the cutoff values of protons and heavy ions. Another method of scaling, namely by subtracting L_{C_P} from L, makes no significant difference in the measured charge states.

The scaled and normalized $f_{ij}(l)$-profiles, with $l = L/L_{C_P}$, are averaged over many orbits. The profiles are then smoothed with a running average, and the cutoff, $l_{C_{ij}}$, is taken at the smallest l with flux above 50% of the mean polar flux ($l > 1.2$). The uncertainty, $\Delta l_{C_{ij}}$, is calculated from the statistical weight of the pulse-height events contributing to the polar flux mean, the difference between the maximal value in the $f_{ij}(l)$-profile and the mean polar flux, and the slope at the cut-off. Examples of smoothed $f_{ij}(l)$-profiles of He, O, and Fe are shown in Figure 2.

In a dipole magnetic field, the inverse square of the geomagnetic cutoff, L_C, is linearly related to the magnetic rigidity, R (see e.g., Smart & Shea 1994); however, for the relatively low rigidities considered here, the cutoffs occur at lower latitudes than are predicted by the linear relationship. As a way of correcting for this and parameterizing the data, we add a constant b' to the equation of Smart & Shea:

$$\frac{1}{L_C^2} = a'R + b' , \tag{1}$$

where the constants a' and b' are determined empirically by a fitting procedure.

We fit a set of straight lines, one for each element, with a common intercept, to the data. Because of the multiplicative scaling, this can be performed with the scaled cutoff values, $l_{C_{ij}}$. As we do not directly measure the rigidity of the particles but only their mass, M_i, and the mean kinetic energy, E_{ij}, of each energy bin, j, we can calculate the product of charge, Q_i, and rigidity, R_{ij}, for each energy bin

$$Q_i R_{ij} = p_{ij} c = \sqrt{(2M_i c^2 + E_{ij})E_{ij}} , \tag{2}$$

where p_{ij} is the momentum of the particles and c is the speed of light.

The linear relation we use for fitting becomes

$$\frac{1}{l_{C_{ij}}^2} = aR_{ij} + b = a_i Q_i R_{ij} + b = a_i\sqrt{(2M_i c^2 + E_{ij})E_{ij}} + b , \tag{3}$$

with the common intercept, b, and the slope, a_i, for each element, i (the product $a_i Q_i = a$ is constant). Each data point, ij, is weighted with the uncertainty $\Delta 1/l_{C_{ij}}^2$, calculated from $\Delta l_{C_{ij}}$. Figure 3 shows data points and the linear fits for some of the more abundant SEP elements, including a single point for the PET protons (at R_P). It can be seen that the relationship given by equation (1) is reasonable for the energy range of the data, since each element is organized roughly along a line of equal charge.

The mean charge of each element, Q_i, can then be calculated from the slopes, a_i, with the constant, a, determined from the relative cutoff, $l_{C_P} = 1$, and the rigidity, R_P, of the 19–28 MeV protons:

$$Q_i = \frac{a}{a_i} , \quad \text{with } a = \frac{[(1/l_{C_P}^2) - b]}{R_P} . \tag{4}$$

The ionization temperature, T_i is calculated from Q_i with tables given in Arnaud & Rothenflug (1985) and Arnaud & Raymond (1992).

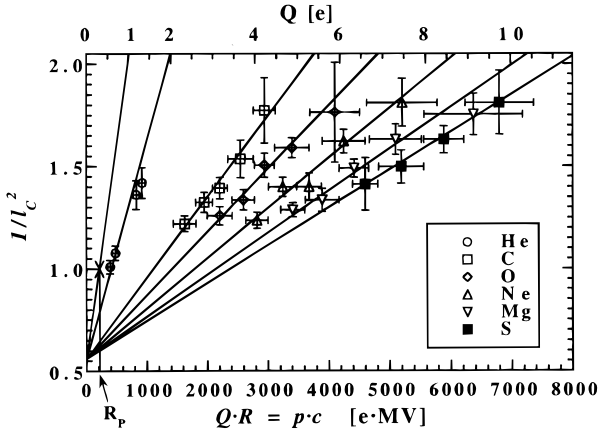

FIG. 3.—Linear relation between the inverse square of the scaled cutoff value and $Q_i R_{ij}$ for some of the more abundant SEP elements. Each data point represents an energy bin of a specific element measured with HILT from 1992 October 31 to November 7.

4. THE MEAN CHARGE OF SEP MEASURED WITH HILT

We present results obtained with the HILT sensor during the time period 1992 October 31–November 7, covering two SEP events with high interplanetary particle intensities. For most of the measured species, the geomagnetic flux cut-off could be determined for five energy bins with a corresponding accuracy in charge of better than 10% over an energy range of ~10–50 MeV per nucleon. For some elements, a few additional bins at higher energies with a larger uncertainty in charge were used as well. The common intercept, b, of the straight lines (eq. [3]), was calculated from the elements with the smallest uncertainties (He, C, O, Ne, Mg, and S). All species were then fitted with straight lines with the fixed intercept, b, to determine the slopes, a_i, and the charge, Q_i (eq. [4]). The mean charge, Q_{ij}, of individual energy bins, E_{ij}, of an element, i, can be calculated from the

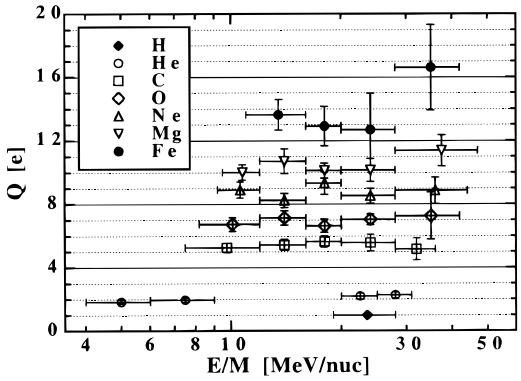

FIG. 4.—Mean charge as a function of energy for the most abundant SEP species measured with HILT from 1992 October 31 to November 7. The horizontal bars represent the width of the energy bins. The proton and helium data points are included to display their energy range.

cutoff, $L_{C_{ij}}$, with a, b, using

$$Q_{ij} = \frac{p_{ij}c}{R_{ij}} = \frac{\sqrt{(2M_i c^2 + E_{ij})E_{ij}}}{[(1/l_{C_{ij}}^2) - b]}\, a\,. \qquad (5)$$

In Figure 4, Q_{ij} is plotted for different energy bins j of the most abundant SEP elements. The mean charge, Q_i, is listed in Table 1 for all observed species i together with the deduced ionization temperature T_i. The temperature is calculated from the mean charge with tables given by Arnaud & Rothenflug (1985) and Arnaud & Raymond (1992). These temperature calculations assume equilibrium charge state distributions. The values in parentheses in column (3) give the range of uncertainty of T_i determined from the uncertainty of Q_i.

TABLE 1

MEAN CHARGE AND IONIZATION TEMPERATURE OF SEP FOR THE TWO EVENTS DURING 1992 OCTOBER 31–NOVEMBER 7 MEASURED WITH HILT

Element i (1)	Mean Charge $Q_i(e)$ (2)	Ionization Temperature $T_i(10^6$ K) (3)
Helium.....	2.0 ± 0.2	...
Carbon	5.4 ± 0.3	1.3 (1.1–1.5)
Nitrogen.....	5.9 ± 0.7	1.6 (1.0–2.2)
Oxygen	6.9 ± 0.3	2.4 (2.0–2.7)
Neon.....	8.7 ± 0.4	4.0 (3.2–5.0)
Magnesium.....	10.4 ± 0.5	5.6 (1.9–8.0)
Silicon	11.0 ± 1.2	1.9 (1.5–8.0)
Sulfur	11.4 ± 0.7	2.2 (2.0–2.4)
Argon.....	10.5 ± 1.7	1.8 (1.1–2.7)
Calcium	11.4 ± 1.7	2.0 (0.8–3.0)
Iron	13.8 ± 1.7	2.0 (1.7–3.1)

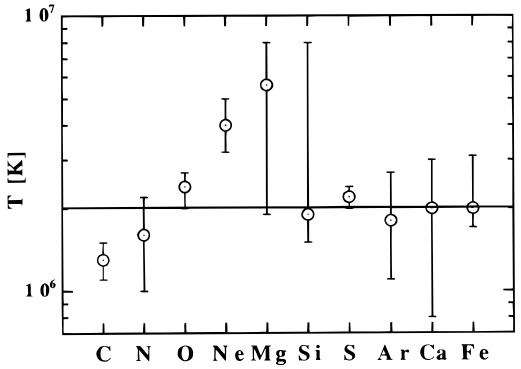

FIG. 5.—Ionization temperature of SEP deduced from the HILT charge state values at energies of 10–50 MeV per nucleon measured during 1992 October 31–November 7.

5. COMBINATION OF THE LICA, HILT, AND MAST RESULTS

The LICA, HILT, and MAST mean charge measurements cover the SEP energy range of 0.3–70 MeV per nucleon. The charge determination was performed independently for each sensor. In all three cases, the mean charge was deduced from the geomagnetic cut-off based on particles with known charge (protons and helium).

With LICA, the mean charge of SEP was measured for C, N, O, Ne, Mg, Si, S, Ca, and Fe with energies 0.3–10 MeV per nucleon (Mason et al. 1995). The cutoff rigidity relation was established with PET protons and LICA helium (assuming fully stripped helium) that cover the complete energy range of the heavy elements measured with LICA.

The data obtained with the MAST sensor cover the energy range 15–70 MeV per nucleon for C, N, O, Ne, Na, Mg, Al, Si, S, Ar, Ca, Fe, and Ni (Leske et al. 1995). The MAST count statistics were sufficient to treat the two SEP events separately; the charge values of the two events are similar. As in the case of HILT, the proton and helium data cover only the lower part of the energy range, and the cutoff–rigidity relation had to be extrapolated to higher values with the linear relation between inverse square of the L-value of the cutoff and rigidity (eq. [1]).

Figure 6 shows the charge states of the most abundant elements as a function of kinetic energy per nucleon and Figure 7 as a function of magnetic rigidity, using the ioniza-

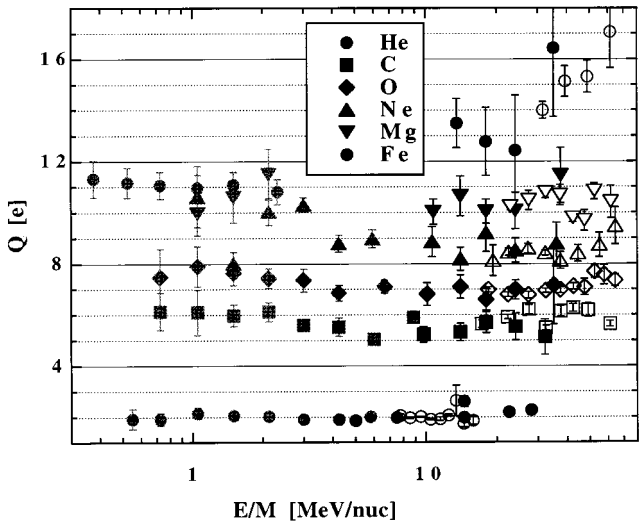

FIG. 6.—SEP charge states for all the energy bins of the three sensors LICA (*gray symbols*), HILT (*black symbols*), and MAST (*open symbols*) during the 1992 October–November events.

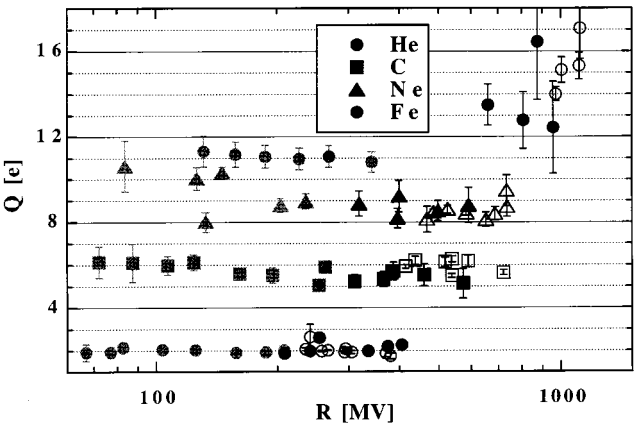

FIG. 7.—SEP charge states vs. rigidity for LICA (*gray symbols*), HILT (*black symbols*), and MAST (*open symbols*) during the 1992 October–November events.

tion values presented here. The ionization values are essentially independent of energy or rigidity, except for Fe, which increases from a value of ~ 11 below a few MeV per nucleon to ~ 16 near 60 MeV per nucleon. The charges averaged over all energy bins of each sensor are displayed in Figure 8, together with the values measured by Luhn et al. (1984), and are listed in Table 2.

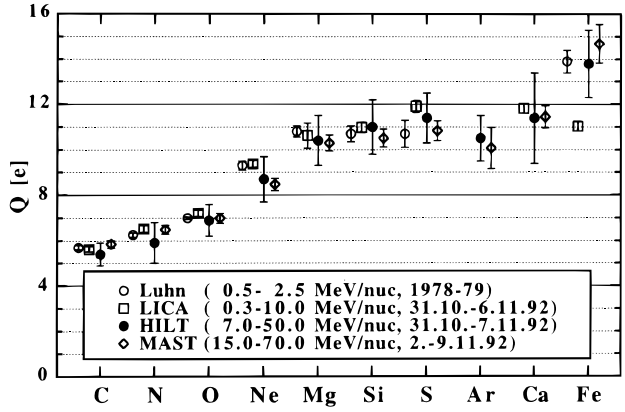

FIG. 8.—Mean ionic charge of SEP measured with LICA, HILT, and MAST during the 1992 October–November events compared with the results of Luhn et al. (1984).

5.1. *Comparison with Other Measurements*

The mean charge states determined here agree well with the earlier survey of Luhn et al. (1984, 1985a), with the exception of Fe. Luhn found a value of $Q_{Fe} = 14.09 \pm 0.09$ around 1 MeV per nucleon, whereas in the current work we find $Q_{Fe} \approx 11$ at low energies, increasing to >16 at energies >50 MeV per nucleon. At even lower energies, Gloeckler et al. (1976) found $Q_{Fe} = 11.6$ over the energy interval ~ 10–250 keV per nucleon in the ^{3}He-rich solar particle event of 1974 May 14–15, and a later analysis by Ma Sung et al. (1981) showed Fe charge states of $+11$–12 as well as $+16$–18 in this same event. These lower Fe ionization states in a ^{3}He-rich solar particle event contrast with the survey of Luhn et al. (1985b), who found $Q_{Fe} = 20.6 \pm 1.2$ in events observed over the period 1978 September–1979 October. At much higher energies, Tylka et al. (1995) found a charge state of Fe of 14.2 ± 1.4 at 200–600 MeV per nucleon in a series of very large solar particle events during 1989 September–October.

5.2. *Mean Charge States and Ionization Temperatures*

The ionization temperatures calculated from the mean charges are essentially the same for all three sensors, as shown in Figure 5 for HILT. The value for all elements is $\sim 2 \times 10^6$ K except for Ne and Mg, which have a significantly higher temperature, and C, which has a somewhat lower temperature.

Neon and especially magnesium have the largest variation of T with Q around 2×10^6 K owing to a large step of the ionization energy at that temperature. The relations between mean charge and temperature given in Arnaud & Rothenflug (1985), and for iron in Arnaud & Raymond (1992), are plotted in Figure 9. The circles mark the elements Ne and Mg at 2×10^6 K. Any nonthermal process that produces higher charge states (e.g., ionization by X-rays [Mullan & Waldron 1986] and suprathermal electrons) causes a highly increased apparent temperature for these species.

Carbon is the only one of the measured elements that just reaches full ionization at 2×10^6 K. Its calculated temperature is therefore most sensitive to any recombination process while being the least sensitive to the nonequilibrium ionization processes mentioned above, which results in a

TABLE 2

MEAN CHARGE OF SEP MEASURED WITH LICA, HILT, AND MAST ON *SAMPEX* DURING THE 1992 OCTOBER–NOVEMBER EVENTS

Element	LICA	HILT	MAST Event 1	MAST Event 2
Helium.....	2.00 ± 0.04	2.0 ± 0.2	1.97 ± 0.07	2.00 ± 0.01
Carbon	5.63 ± 0.11	5.4 ± 0.3	5.86 ± 0.17	5.85 ± 0.17
Nitrogen.....	6.52 ± 0.16	5.9 ± 0.7	6.30 ± 0.30	6.49 ± 0.20
Oxygen	7.21 ± 0.15	6.9 ± 0.3	6.93 ± 0.20	6.99 ± 0.22
Neon.....	9.38 ± 0.16	8.7 ± 0.4	8.68 ± 0.30	8.47 ± 0.29
Sodium	...	...	8.50 ± 0.39	9.36 ± 0.37
Magnesium.....	10.62 ± 0.55	10.4 ± 0.5	10.35 ± 0.40	10.29 ± 0.35
Aluminum.....	...	...	11.63 ± 0.73	10.66 ± 0.68
Silicon	10.98 ± 0.23	11.0 ± 1.2	10.57 ± 0.39	10.51 ± 0.40
Sulfur	11.91 ± 0.25	11.4 ± 0.7	10.82 ± 0.81	10.84 ± 0.44
Argon.....	...	10.5 ± 1.7	...	10.08 ± 0.91
Calcium	11.83 ± 0.21	11.4 ± 1.7	...	11.46 ± 0.49
Iron	11.04 ± 0.22	13.8 ± 1.7	15.59 ± 0.81	14.69 ± 0.86
Nickel.....	...	...	11.63 ± 0.73	10.66 ± 0.68

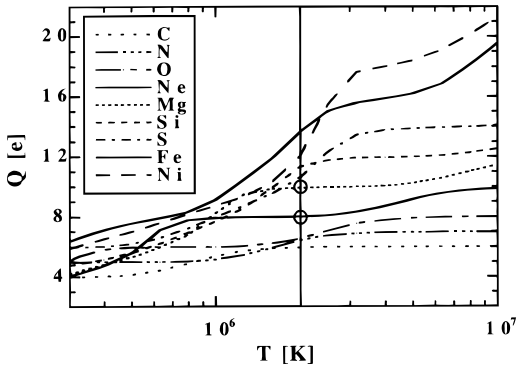

FIG. 9.—Relation between mean charge, Q, and ionization temperature, T, for equilibrium conditions (Arnaud & Rothenflug 1985; Arnaud & Raymond 1992).

value rather below 2×10^6 K. Iron has the steepest $Q(T)$ curve; variations in the measured charge have the smallest influence on the calculated temperature. A variation in charge of $+11$ to $+15$ gives a variation in temperature of $1.5–2.5 \times 10^6$ K for iron.

5.3. *Energy Dependence of the Fe Ionization State*

Figures 6 and 7 show that all the elements, except for Fe, have ionization states that are essentially independent of energy over the large energy range 0.3–70 MeV per nucleon. There are several properties of Fe that are unique in this data set, and these may result in an energy dependence of Fe charge states that is not observed for the other elements. The most important difference separating Fe from the other species can be seen in Figure 9, which shows that species lighter than Fe are much less sensitive to variations in temperature than Fe, since their ionization curves are nearly flat over a broad range near the $\sim 2 \times 10^6$ K typical value deduced from our measurements. Fe stands out as having an ionization state that changes sensitively over most of the temperature range shown, and thus the ionization state of Fe is the most sensitive indicator of the temperature history of the particles covered in this study. Given this higher sensitivity, it could be expected that any energy dependence of the ionization states would be seen most strongly in Fe and less, if at all, in lighter species. Below, we discuss mechanisms that could cause an energy dependence in the Fe ionization state.

5.3.1. *Differing Seed Populations*

Numerous lines of evidence suggest that large solar energetic particle events such as the ones studied here are best explained by a mechanism in which the seed particles are accelerated by large-scale shocks in the outer corona and beyond (see, e.g., Mason, Gloeckler, & Hovestadt 1984; Lin 1987; Cane, Reames, & von Rosenvinge 1988; Gosling 1993). Particle fluxes measured at 1 AU are thus the result of an acceleration process that is distributed in space and time. Over the large range of energies studied here, these processes yield different behaviors as can be seen from Figure 1, which shows Fe fluxes at 0.25 MeV per nucleon and 2.4 MeV per nucleon and O at 18.1 MeV per nucleon for the particle events. At the higher energies, two separate solar particle events stand out clearly, and the shock on day 308 is a small perturbation on the ambient fluxes. At low energies, the second solar particle event cannot be clearly identified, and the shock on day 308 produces a very large perturbation on the ambient fluxes. Interpreted in the context of the large-scale shock models cited above, this behavior would indicate that the high-energy particles were accelerated near the Sun, early in the event, while at the lowest energies, much or most of the acceleration took place by the shock in interplanetary space.

In this case, the lower energy particles may have ionization states more typical of solar wind values, which are in the range $\sim 11–12$ (Ipavich et al. 1992; Galvin et al. 1995), similar to the low-energy values found here. At the higher energies, the Fe charge states may be indicative of a region closer to the flare site that had higher temperatures or that had been subjected to other processes such as ionization by X-rays (Mullan & Waldron 1986).

5.3.2. *Rigidity Dependence in the Acceleration Mechanism*

Acceleration in large solar particle events has often been modeled in terms of diffusive particle acceleration such as could be expected to take place at the coronal and interplanetary shocks associated with these events and in terms of stochastic acceleration in regions with increased wave turbulence (see, e.g., Ellison & Ramaty 1985; Forman, Ramaty, & Zweibel 1986; Miller, Guessoum, & Ramaty 1990). Mazur et al. (1992) have carried out a study of heavy-ion abundances in 10 large solar particle events and have compared the spectral forms with results of a stochastic acceleration model based on earlier work by Möbius et al. (1982). These models, which result in Bessel functions, gave good fits to the measured spectra. The solar particle events in Mazur et al. (1992) had Fe/O ratios that showed significantly different behavior from event to event: The ratio often decreased with increasing energy; however, in some events, there was little energy dependence in this ratio (i.e., the spectra were of the same shape), and in one case (1977 November 22), it increased with increasing energy. In the events studied here, the Fe/O ratio decreases with increasing energy: near 1 MeV per nucleon, the average for the two events is Fe/O $= 0.41 \pm 0.03$ (Mason et al. 1995), while in the range $\sim 20–70$ MeV per nucleon, the ratio was Fe/O $= 0.031 \pm 0.007$ (event 1) and Fe/O $= 0.071 \pm 0.006$ (Selesnick et al. 1993). Taking the average of the two higher energy measurements, the Fe/O ratio decreased by a factor of 8 over the energy range covered in Figure 7.

This very substantial decrease in the Fe/O ratio is consistent with an acceleration process that was less effective at accelerating high rigidity (i.e., low charge-to-mass ratio) particles than low-rigidity particles. This type of behavior could be well fitted by stochastic models as shown by Mazur et al. (1992). In addition, the energy spectra in the SEP events fall very steeply at high energy, which leads to a near cut-off of the spectrum. If the seed population of Fe ions being accelerated included a broad range of ionization states, as shown by the solar wind studies cited above, then at the high-energy portion of the spectrum, particles with high ionization states would be favored since their rigidity was lower. This could lead to a more efficient acceleration of high charge state ions in the range above a few tens of MeV per nucleon, which is consistent with the trend found in the present study.

A model calculation according to Brenemann & Stone (1985) for the dependence of the mean charge of iron on the Fe/O ratio is shown in Figure 10 (*solid line*). The four data

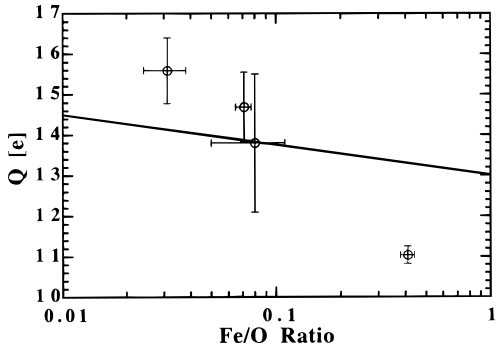

FIG. 10.—Charge of iron SEP as a function of Fe/O ratio measured and modeled (*solid line*) according to Brenemann & Stone (1985).

points display the values measured with MAST (two leftmost symbols for the two observed events), HILT, and LICA. The model, described in Mewaldt & Stone (1989), uses a charge per mass-dependent acceleration process that assumes the accelerated abundance ratio, N_i/N_j, of two ion species, i and j, to be related to their source abundance ratio S_i/S_j as a power law in (Q/M) with an index α:

$$\frac{N_i}{N_j} = \left(\frac{Q_i/M_i}{Q_j/M_j}\right)^{\alpha} \frac{S_i}{S_j} . \tag{6}$$

The charge state ratios, N_{Q_i}/N_{Q_j}, and therefore the mean charge of accelerated iron can then be deduced from the source charge state ratios of iron in the corona, S_{Q_i}/S_{Q_j}, using the change of the iron-to-oxygen ratio $(\mathrm{Fe/O})_{\mathrm{acc}}/(\mathrm{Fe/O})_{\mathrm{cor}}$:

$$\frac{N_{Q_i}}{N_{Q_j}} = \left(\frac{Q_i}{Q_j}\right)^{\alpha} \frac{S_{Q_i}}{S_{Q_j}} , \quad \text{with } \alpha = \frac{\ln(\mathrm{Fe/O})_{\mathrm{acc}} - \ln(\mathrm{Fe/O})_{\mathrm{cor}}}{\ln(Q/M)_{\mathrm{Fe}} - \ln(Q/M)_{\mathrm{O}}} . \tag{7}$$

For the source charge state distribution of iron as well as for the charge per mass of oxygen and iron, we assumed an equilibrium distribution at 2×10^6 K. For the source abundance ratio in the corona, we assumed $(\mathrm{Fe/O})_{\mathrm{cor}} = 0.17$, and for the accelerated abundance ratio $(\mathrm{Fe/O})_{\mathrm{acc}}$, we used our measurements.

The calculation indicates the trend but cannot explain the magnitude of the dependence over the energy range presented here, which extends to considerably lower energies than the Brenemann & Stone study.

We thank the dedicated members of the participating institutes who designed, constructed, and calibrated the HILT, LICA, MAST, and PET instruments. We are particularly grateful to the Small Explorer Project Office and the Orbiting Satellites Branch at Goddard Space Flight Center for the construction, launch, and postlaunch operation of the *SAMPEX* spacecraft. This work was supported by the Bundesministerium für Forschung und Technologie, Germany, grant number 50 OC90021 and by NASA, contract, NAS 5-30704, and grant NAG-2963.

REFERENCES

Arnaud, M., & Raymond, J. 1992, ApJ, 398, 394
Arnaud, M., & Rothenflug, R. 1985, A&AS, 60, 425
Baker, D. N., Mason, G. M., Figueroa, O., Colon, G., Watzin, J. G., & Aleman, R. M. 1993, IEEE Trans. Geosci. Remote Sensing, 31, 531
Brenemann, H. H., & Stone, E. C. 1985, ApJ, 299, L57
Cane, H. V., Reames, D. V., & von Rosenvinge, T. T. 1988, J. Geophys. Res., 93, 9555
Cook, W. R., et al. 1993a, IEEE Trans. Geosci. Remote Sensing, 31, 557
———. 1993b, IEEE Trans. Geosci. Remote Sensing, 31, 565
Ellison, D. C., & Ramaty, R. 1985, ApJ, 298, 400
Forman, M. A., Ramaty, R., & Zweibel, E. G. 1986, in Physics of the Sun, Vol. II, ed. P. A. Sturrock (Dordrecht: Reidel), 249
Galvin, A. B., Ipavich, F. M., Cohen, C. M. S., Gloeckler, G., & von Steiger, R. 1995, Space Sci. Rev., 72, 65
Gloeckler, G., Sciambi, R. K., Fan, C. Y., & Hovestadt, D. 1976, ApJ, 209, L93
Gloeckler, G., et al. 1981, 17th Internat. Cosmic Ray Conf. (Paris), 3, 136
Gosling, J. T. 1993, J. Geophys. Res., 98, 18937
Hovestadt, D., et al. 1981, Adv. Space Res., 1, 61
Ipavich, F. M., Galvin, A. B., Geiss, J., Ogilvie, K. W., & Gliem, F. 1992, in Solar Wind Seven, ed. E. Marsch & R. Schwenn (Oxford: Pergamon Press), 369
Klecker, B., Hovestadt, D., Gloeckler, G., Möbius, E., Ipavich, F. M., & Scholer, M. 1983, 18th Internat. Cosmic Ray Conf. (Bangalore), 4, 65
Klecker, B., Hovestadt, D., Gloeckler, G., Ipavich, F. M., Scholer, M., Fan, C. Y., & Fisk, L. A. 1984, ApJ, 281, 458
Klecker, B., et al. 1993, IEEE Trans. Geosci. Remote Sensing, 31, 542
Leske, R. A., Cummings, J. R., Mewaldt, R. A., Stone, E. C., & von Rosenvinge, T. T. 1995, ApJ, 452, L149
Lin, R. P. 1987, Rev. Geophys., 25, 676
Luhn, A., Klecker, B., Hovestadt, D., Gloeckler, G., Ipavich, F. M., Scholer, M., Fan, C. Y., & Fisk, L. A. 1984, Adv. Space Res., 4, 161
Luhn, A., et al. 1985a, 19th Internat. Cosmic Ray Conf. (La Jolla) (NASA CP-2376), 4, 241
Luhn, A., Klecker, B., Hovestadt, D., & Möbius, E. 1985b, 19th Internat. Cosmic Ray Conf. (La Jolla) (NASA CP-2376), 4, 285
———. 1987, ApJ, 317, 951
Mason, G. M., Gloeckler, G., & Hovestadt, D. 1984, ApJ, 280, 902
Mason, G. M., Hamilton, D. C., Walpole, P. H., Heuermann, K. F., James, T. L., Lennard, M. H., & Mazur, J. E. 1993, IEEE Trans. Geosci. Remote Sensing, 31, 549
Mason, G. M., Mazur, J. E., Looper, M. D., & Mewaldt, R. A. 1995, ApJ, 452, 901
Ma Sung, L. S., Gloeckler, G., Fan, C. Y., & Hovestadt, D. 1981, ApJ, 245, L45
Mazur, J. E., Mason, G. M., Klecker, B., & McGuire, R. E. 1992, ApJ, 401, 398
Mewaldt, R. A., & Stone, E. C. 1989, ApJ, 337, 959
Miller, J. A., Guessoum, N., & Ramaty, R. 1990, ApJ, 361, 701
Möbius, E., Scholer, M., Hovestadt, D., Klecker, B., & Gloeckler, G. 1982, ApJ, 259, 397
Mullan, D. J., & Waldron, W. L. 1986, ApJ, 308, L21
Selesnick, R. S., Cummings, A. C., Cummings, J. R., Leske, R. A., Mewaldt, R. A., Stone, E. C., & von Rosenvinge, T. T. 1993, 23d Internat. Cosmic Ray Conf. (Calgary), 3, 392
Smart, D. F., & Shea, M. A. 1994, Adv. Space Res., 14, 787
Tylka, A. J., Boberg, P. R., Adams, J. H., Jr., Beahm, J. P., & Dietrich, W. F. 1995, ApJ, 444, L109